World Journal of Advanced Engineering Technology and Sciences
eISSN: 2582-8266
Cross Ref DOI: 10.30574/wjaets
Journal homepage: https://wjaets.com/

(RESEARCH ARTICLE)

Check for updates

Fracture Surface Morphology and Mechanical Performance of Al7075 Composites Reinforced with B_4C, Gr and ZrO_2 particles

Sampath Kumar R. [1, 2, *] and H. C. Chittappa [2]

[1] *Selection Grade-1 Lecturer, Department of Mechanical Engineering, Government Polytechnic Hosadurga-577527, Karnataka, India.*
[2] *Department of Mechanical Engineering, University Visvesvaraya College of Engineering, Bangalore University, Bangalore-560001, Karnataka, India.*

World Journal of Advanced Engineering Technology and Sciences, 2025, 17(03), 491-502

Publication history: Received on 24 November 2025; revised on 29 December 2025; accepted on 31 December 2025

Article DOI: https://doi.org/10.30574/wjaets.2025.17.3.1569

Abstract

This study investigates the mechanical behaviour and fractographic properties of Al-7075 metal matrix composites that are individually reinforced with 3 weight percent boron carbide (B_4C), graphite (Gr), and zirconia (ZrO_2) using a two-step stir-casting. To assess the impact of specific reinforcements on mechanical response and fracture processes, three composite systems were created, Al7075+B_4C, Al7075+Gr, and Al7075+ZrO_2. Strong interfacial bonding with the aluminium matrix and uniform reinforcement dispersion were verified by microstructural characterization using energy dispersive spectroscopy (EDS) and scanning electron microscopy (SEM). Tensile and hardness tests were used to assess the mechanical behaviour of the composites. Compression- and impact-fractured specimens were then subjected to in-depth fractographic examination to determine the predominant failure mechanisms. The B_4C-reinforced composite exhibited enhanced strength and load-bearing capacity, reflected by brittle cleavage features and reduced plastic deformation. In contrast, the graphite-reinforced composite demonstrated improved toughness, characterized by ductile fracture behaviour with pronounced dimpling and effective crack deflection. The ZrO_2-reinforced composite displayed mixed-mode fracture characteristics, governed by localized plastic deformation and particle–matrix interfacial debonding. The novelty of this work lies in the direct comparative evaluation of mechanical behaviour and fracture surface morphology of Al-7075 composites reinforced with B_4C, Gr, and ZrO_2 at an identical reinforcement content, providing insight into the structure–property relationships of individually reinforced Al-7075 composites.

Keywords: Al7075; Metal Matrix Composite; fracture; Microstructure; Boron Carbide; Graphite; Zirconia

1. Introduction

Contemporary engineering applications in aerospace, defence, automotive, and recreational sectors demand materials that combine high strength, low weight, cost efficiency, and versatile properties, which are challenging to achieve with conventional monolithic materials [1]. Among the different classes of composites, metal matrix composites (MMCs) are preferred for applications requiring enhanced mechanical strength, thermal stability, and wear resistance. Aluminium-based MMCs (AMCs), in particular, are widely employed in aerospace, marine, and automotive industries due to their lightweight and high-performance characteristics [2–3]. Aluminium-based metal matrix composites (AMCs) can be synthesized using a variety of methods depending on their intended applications. To fulfill the demanding requirements of high-strength, lightweight, and wear-resistant materials, several manufacturing approaches and alternative reinforcement strategies have been explored. Among these, liquid-state processing (casting) and solid-state processing (powder metallurgy) are the most widely employed techniques for producing aluminium composites due to their versatility, scalability, and ability to achieve uniform reinforcement distribution [4–7].The combination of aluminium

* Corresponding author: Sampath Kumar R.

with various particulate reinforcements, such as Al_2O_3, B_4C, fly ash, and ZrO_2, enhances properties including wear resistance, stiffness, and tensile strength [8,9]. B_4C is recognized as an ideal reinforcement for aluminium composites because of its high hardness, low density, and strong chemical and thermal stability, surpassing traditional ceramic reinforcements such as Al_2O_3 and SiC [10-12]. In order to engineer aluminium composites with desired characteristics, diverse reinforcing particles have been utilized. Among these, graphite is widely adopted to improve the frictional and wear performance of the material [13]. Al-6061/ZrO_2 composites with 3 wt.% ZrO_2 showed uniform particle distribution, fine grains, and improved hardness, wear, and corrosion resistance, while higher contents (>6 wt.%) caused agglomeration and reduced performance, making 3 wt.% optimal [14]. Al-7075/SiC/Gr composites with 2 wt.% graphite showed optimal hardness, wear resistance, and strength–damping balance, while higher graphite reduced hardness [15]. Al/Gr/ZrO_2 composites were prepared via a two-step stir casting process, improving particle distribution, wettability, and interfacial bonding [16-19]. This study evaluates Al-7075 composites reinforced individually with 3 wt.% B_4C, graphite, and ZrO_2 using a two-step stir-casting process, providing a direct comparison of fracture surfaces and wear debris evolution. The findings reveal how each reinforcement influences mechanical performance, fracture behaviour, and wear mechanisms, offering insights for selecting optimal reinforcements for lightweight, high-performance applications in aerospace, automotive, and defence sectors.

2. Experimental Setup and Procedure

2.1. Preparation of Materials and Fabrication of Composites

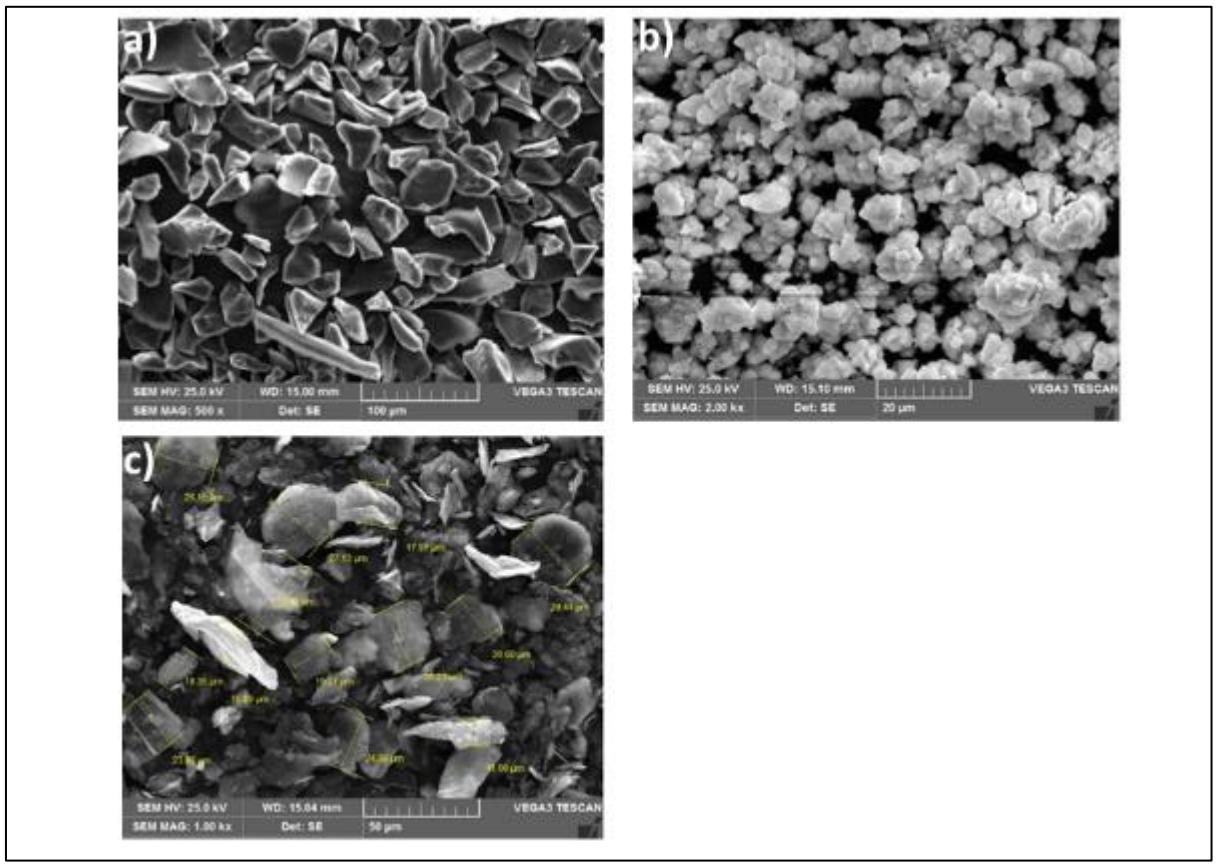

Figure 1 SEM images of reinforcement particles: (a) B_4C, (b) ZrO_2, (c) Graphite

The matrix material was chosen to be Al-7075 aluminium alloy ingots (Perfec Metal Works, Bengaluru, India), a high-strength Al–Zn–Mg–Cu alloy that is frequently used in structural and aerospace applications. Particles of zirconia (ZrO_2, 20–30 μm) and boron carbide(B_4C, 20–35 μm) graphite (Gr, 30–40 μm) were purchased from Speedfam (India) Pvt. Ltd., Chennai, and used as reinforcements. Tables 1 and 2 summarise the essential physical characteristics and chemical makeup of the reinforcement particles and matrix alloy. As shown in Figures 1 and 2, the morphology and elemental composition of the reinforcement particles were investigated using SEM and EDS prior to composite fabrication. These characterisation results validated the reinforcements' suitability for successful integration into the Al-7075 matrix in terms of morphology, chemical purity, and particle size distribution.

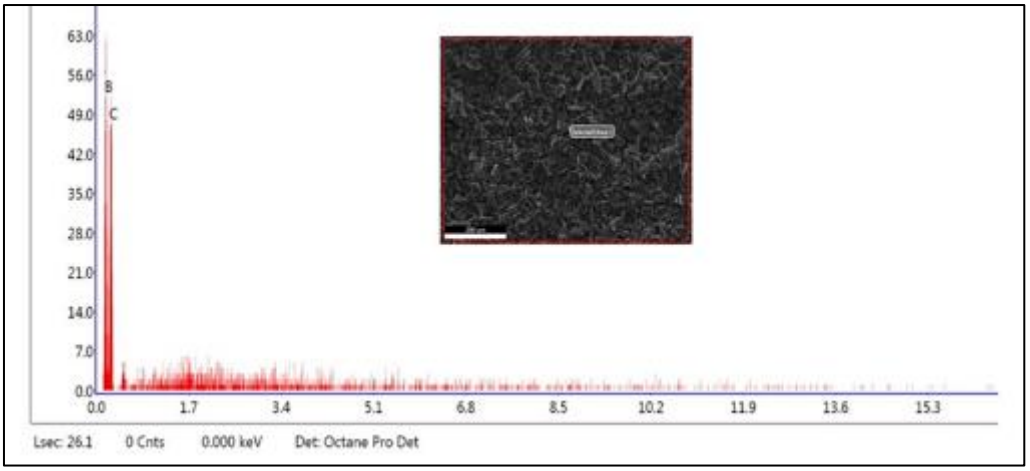

Figure 2a EDS spectrum of Boron Carbide particles

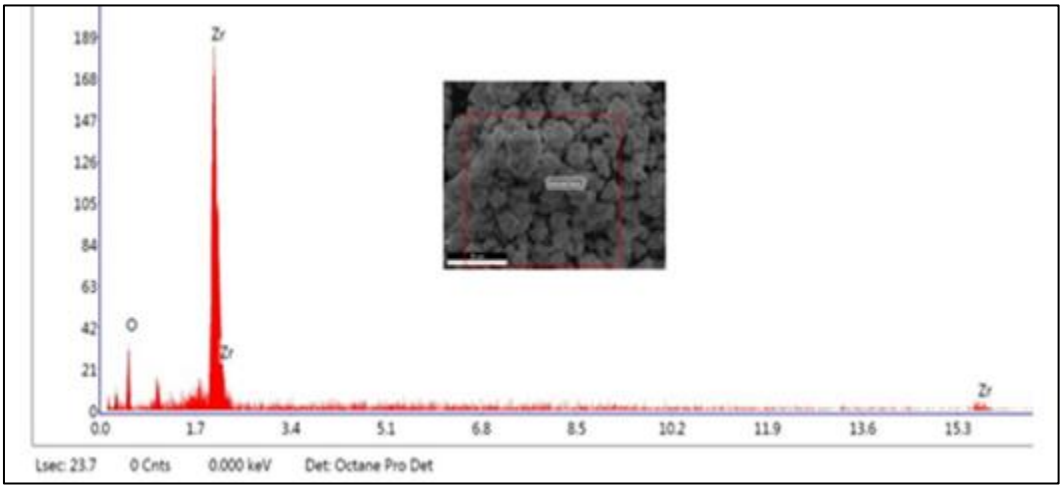

Figure 2b EDS spectrum of ZrO_2 particles

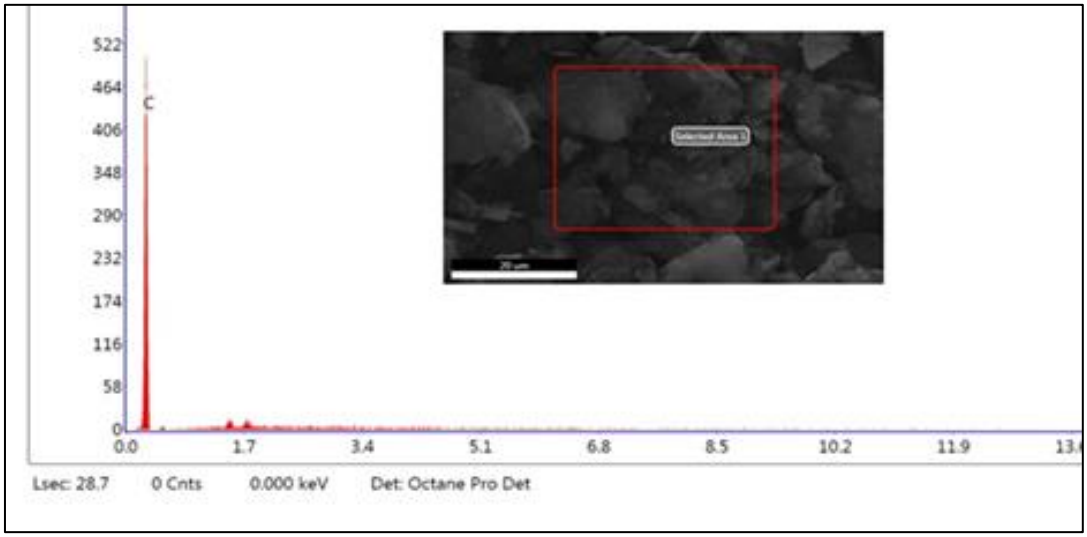

Figure 2c Graphite particle EDS spectrum

Figure 2(a-c) EDS spectra of reinforcements showing boron carbide (carbon 21.69 wt.%, boron 78.31 wt.%), zirconium dioxide (zirconium 67.28 wt.%, oxygen 32.72 wt.%), and graphite (carbon 100 wt.%).

Table 1 Composition of Al7075 Alloy in Weight Percent

Cu	Si	Mg	Cr	Fe	Zn	Mn	Ti	Al
1.95	0.40	2.89	0.22	0.49	6.03	0.26	0.20	Balance

The matrix was made of Al-7075 aluminium alloy, reinforced with 3 weight percent graphite, boron carbide, and zirconia. Al7075–B_4C, Al7075–Gr, and Al7075–ZrO_2 were the names given to the composites.

Table 2 Characteristics of the boron carbide, graphite, ZrO2 particles and Al7075 alloy

Material	Hardness (BHN)	Tensile Strength (MPa)	Density (gm/cm3)	Elastic Modulus (GPa)
Al7075	65	205	2.80	70
Graphite	1.3*	200	2.2	16
ZrO2	1300	1800 (C)**	5.68	380
Boron Carbide	2900	350	2.52	460

*Mohs Hardness **Compression Strength

A common two-step stir-casting technique in liquid metallurgy was used to create the metal matrix composites. Commercial Al7075 alloy was first precisely heated to 650–680 °C in a graphite crucible. The alloy melted completely and steadily thanks to thermal monitoring. To release trapped gases and reduce porosity, the molten metal was then treated with solid hexachloroethane [21].

In the second step, the ceramic reinforcements preheated to 300–350 °C to remove moisture and improve wettability with the molten aluminium. The particles were incorporated into the melt using a controlled two-step addition along with K_2TiF_6 flux to enhance interfacial bonding and ensure uniform dispersion. Continuous mechanical stirring at 300 rpm for 5–10 minutes was applied to prevent agglomeration and achieve homogeneous particle distribution throughout the matrix.

To minimise thermal shock and enhance solidification quality, the composite melt was thoroughly mixed, heated to a regulated pouring temperature of 720–740 °C, and then placed into a warmed cast iron die kept at 200–250 °C. The cast composites were let to cool naturally. The resultant cylindrical samples were appropriate for mechanical testing and had dimensions of 15 mm in diameter and 120 mm in length. Strong interfacial bonding, consistent reinforcement distribution, and few casting flaws were guaranteed by this meticulously regulated two-step casting process.

Figure 3 Stir-casting setup for Al-7075 composite fabrication.

Figure 4 Al-7075 composites reinforced with B_4C, ZrO_2, and graphite.

Figure-3 depicts the stir-casting setup employed for composite fabrication, while figure-4 presents the cast Al-7075 specimens reinforced with B_4C, ZrO_2, and graphite particles. For microstructural examination, the samples were prepared following standard metallographic protocols. Initially, the specimens were successively ground using silicon-carbide papers of 200, 400, 600, and 800 grit to produce a smooth, defect-free surface, then polished on a velvet cloth with a suitable polishing medium to achieve a mirror finish. Polished surfaces were etched with Keller's reagent (a controlled mixture of HNO_3, HF, and HCl) to expose grain boundaries, particle distribution, and matrix–reinforcement interfaces, followed by thorough rinsing with distilled water. SEM analysis using a VEGA3 TESCAN instrument (Fig 5) enabled detailed evaluation of reinforcement dispersion, interfacial bonding, and morphological characteristics critical to the mechanical behavior of the composites.

Hardness specimens were machined and prepared in strict compliance with ASTM E10 [22]. Brinell hardness testing was performed using a calibrated hardness testing apparatus, with the surfaces carefully finished to achieve a uniform, burr-free contact area. A 5 mm diameter steel ball indenter was applied under a 250 kgf load, and three measurements were taken at well-distributed locations on each sample. The average values were reported as the representative Brinell hardness of the material.

Figure 5 SEM/EDAX (VEGA3 TESCAN)

Tensile specimens were prepared according to ASTM E8 [23] to assess the mechanical performance of as-cast Al-7075 and its 3 wt.% particulate-reinforced composites. Uniaxial tensile testing was employed to determine ultimate tensile strength and evaluate the effect of uniform reinforcement incorporation on the stress–strain response and deformation mechanisms of the alloy. Specimens were machined to a total length of 104 mm, a gauge length of 45 mm, and a gauge diameter of 9 mm, as depicted in figure6. The tests enabled quantification of critical mechanical properties and provided detailed insight into the elastic–plastic behavior and load transfer efficiency within the composites.

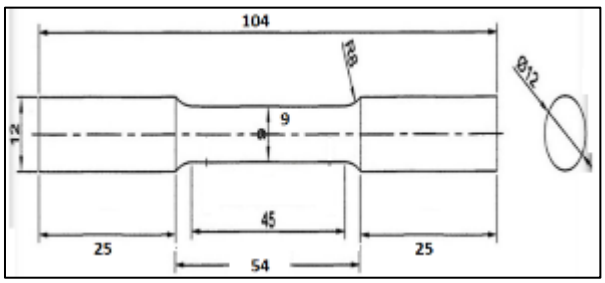

Figure 6 Tensile specimen dimensions as per ASTM standard.

Compressive behavior of Al-7075 and its 3 wt.% particulate-reinforced composites was evaluated in accordance with ASTM E9, as illustrated in figure-7. Cylindrical specimens with a height-to-diameter ratio of 2:1 were subjected to uniaxial compressive loading to determine their compressive strength and deformation characteristics. The tests facilitated assessment of reinforcement uniformity on stress–strain response, load-bearing efficiency, and overall mechanical integrity of the composites.

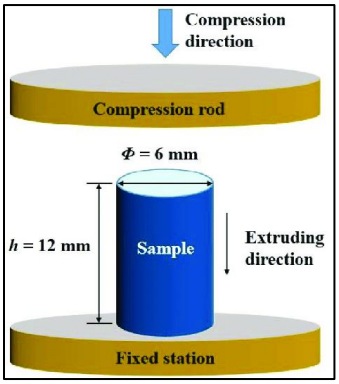

Figure 7 Geometry of compression specimens according to ASTM

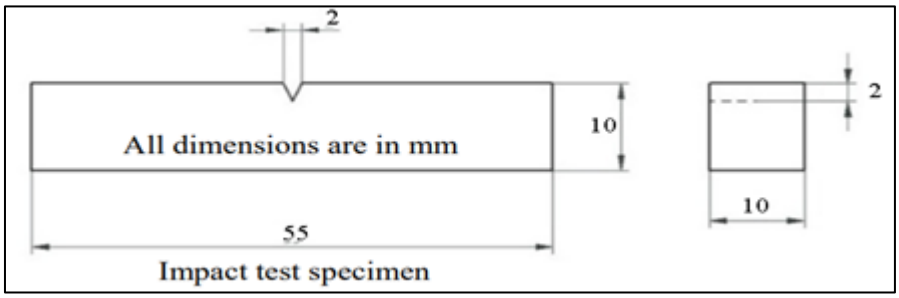

Figure 8 ASTM-compliant Charpy impact specimen dimensions.

The impact testing sample used to assess the fracture toughness of Al-7075 and its particulate-reinforced composites in compliance with ASTM E23 is shown in figure-8. Impact toughness was measured by subjecting notched Charpy specimens to dynamic impact loading and measuring the energy lost during fracture.

3. Experimental Results and Analysis

3.1. Microstructural Analysis

Figure 9a illustrates the microstructural features of the unreinforced Al-7075 alloy, whereas Figures 9(b–d) show the composites reinforced with 3 wt.% B_4C, ZrO_2, and graphite, respectively. The SEM observations indicate a uniform spatial distribution of the reinforcement particulates without noticeable porosity or void formation. The use of a two-step stir-casting route, along with preheating of the reinforcements, enhanced particle wettability and dispersion within the molten matrix. The micrographs further reveal sound matrix–particle interfacial integrity, confirming effective incorporation and strong bonding of B_4C, ZrO_2, and graphite within the Al-7075 matrix.

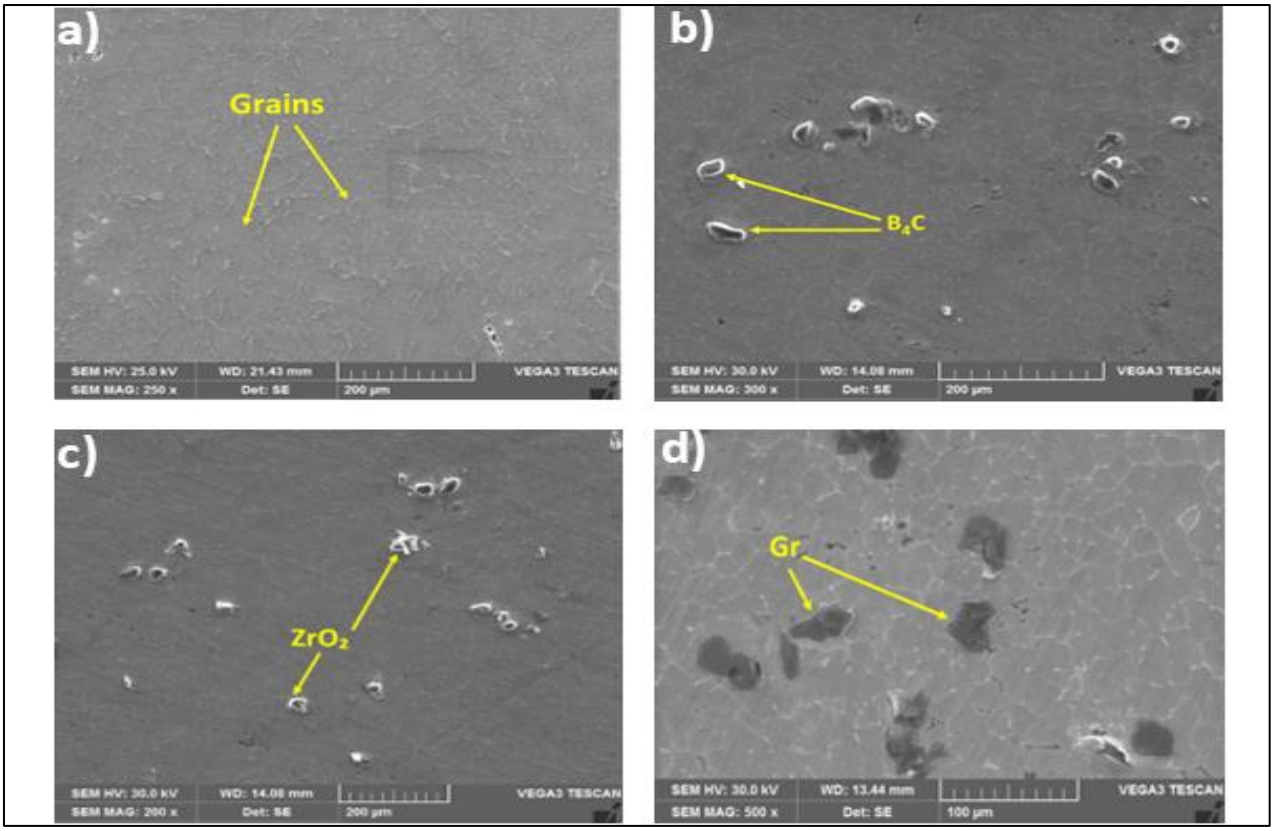

Figure 9 SEM micrographs of (a) As-cast Al-7075 and (b) Al-7075–3 wt.% B_4C (c) Al-7075–3 wt.% ZrO_2 and (d) Al-7075–3 wt.% Gr composites

Figure 10a presents the energy-dispersive X-ray spectroscopy (EDS) profile of the Al-7075 alloy, verifying its chemical composition. Prominent elemental peaks corresponding to Si, Cu, Mn, Ti, Mg, Fe, and Zn are detected, with Zn exhibiting the dominant signal, indicating its significant contribution to the alloy's compositional framework.

Figure 10(b–d) displays the EDS spectra of Al-7075 composites containing 3 wt.% B_4C, ZrO_2, and graphite, respectively. In each spectrum, Zn appears as the most intense peak, highlighting its dominance as the primary alloying constituent of Al-7075. Distinct elemental signatures associated with the reinforcements are also detected, including B and C for B_4C (Fig. 10b), Zr and O for ZrO_2 (Fig. 10c), and C for graphite (Fig. 10d). These compositional features clearly verify the successful incorporation and stable presence of the respective reinforcements within the Al-7075 matrix.

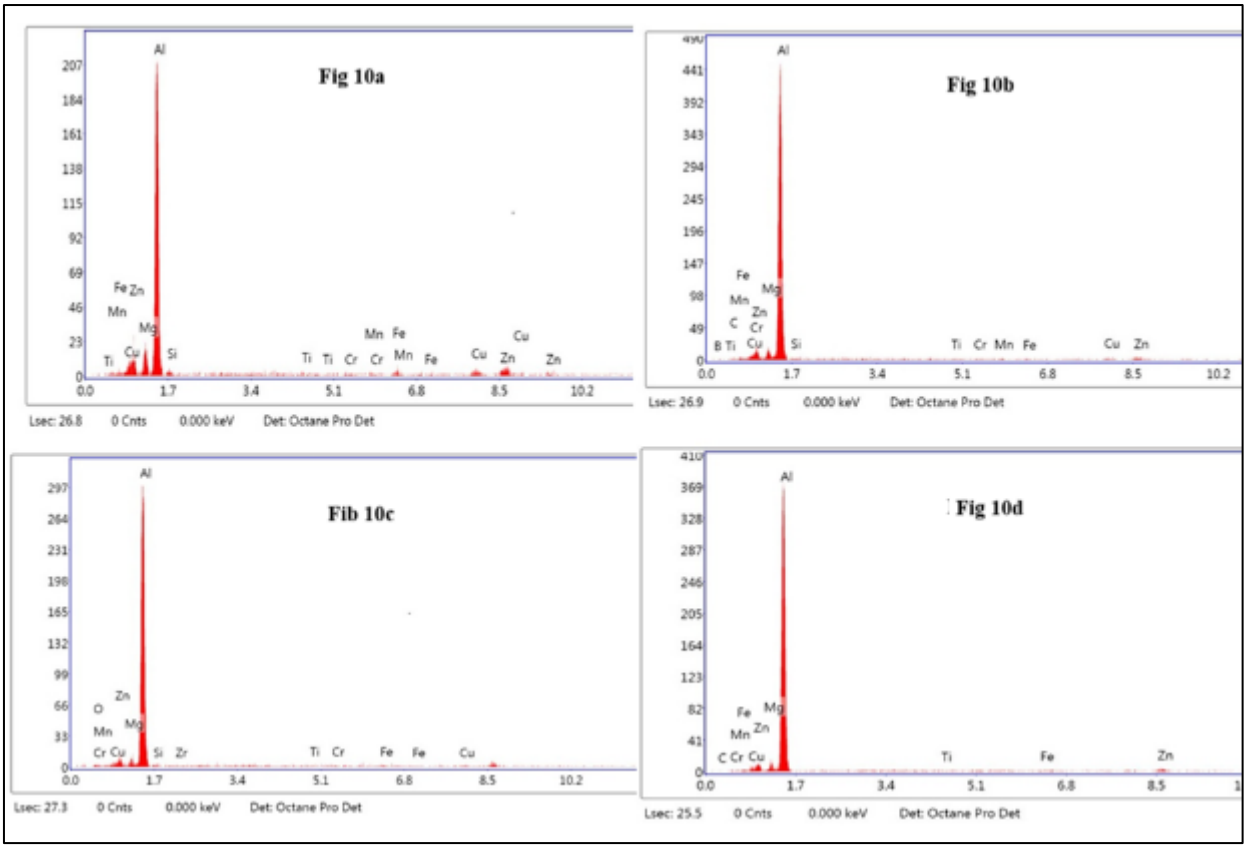

Figure 10 EDS spectra of (a) As cast Al-7075, Al-7075 composites reinforced with 3 wt.% (a) B_4C, (b) ZrO_2, and (c) graphite.

3.2. Hardness

Hardness measurements were performed using a Brinell ball indenter under a 250 kgf load with a dwell time of 30 s, as shown in figure11. The base Al-7075 alloy exhibited a hardness of 68.7 BHN. The addition of 3 wt.% graphite reduced the hardness to 64.0 BHN due to the soft and lubricating nature of graphite, which does not effectively obstruct dislocation motion and instead promotes ductility, consistent with reported literature [24]. In contrast, incorporating 3 wt.% ZrO_2 increased the hardness by approximately 11% owing to grain refinement and the presence of hard ceramic particles that restrict dislocation movement through Orowan strengthening and thermal mismatch effects. The highest hardness improvement was observed for the 3 wt.% B_4C-reinforced composite, where hardness increased to 79.3 BHN (≈15.4%). This enhancement is attributed to the high stiffness of B_4C particles, their uniform dispersion, and strong matrix–particle interfacial bonding, which collectively improve resistance to indentation and wear [25]. In overall, Graphite lowers the hardness of Al-7075 due to its soft, lubricating nature, while ZrO_2 and B_4C enhance hardness through effective strengthening mechanisms, with B_4C providing the maximum improvement.

3.3. Tensile Properties

Figure 11 illustrates how the type of reinforcement has a significant impact on the tensile characteristics of Al-7075 composites. Because graphite reinforcement primarily contributes to crack deflection rather than a significant restriction of dislocation motion, it only slightly increases strength. Because of particle-induced grain refinement and the creation of a more homogeneous microstructure, the addition of ZrO_2 results in a moderate increase in tensile strength. Due to uniform particle dispersion, strong matrix–particle interfacial bonding, and efficient microstructural refinement that improves load transfer and suppresses plastic deformation, the B_4C-reinforced Al-7075 has the highest tensile enhancement of all the composites, achieving a yield strength of 210 Mpa, around 11.5% increase compared to the base alloy As a result, B_4C-reinforced Al-7075 composites are ideal for defence, automotive, and aerospace applications that need exceptional strength and dependability.

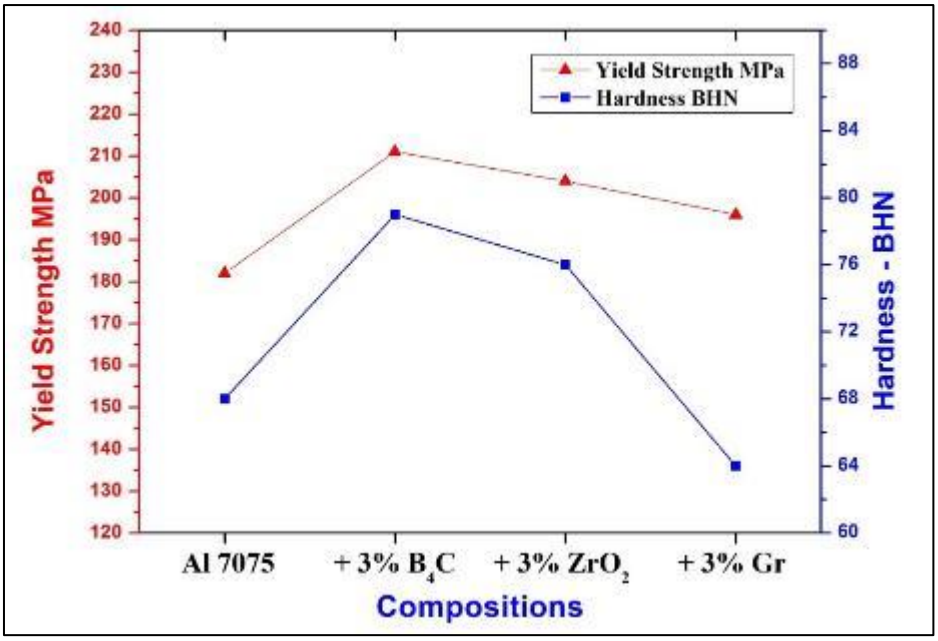

Figure 11 Variation in Hardness and Yield strength of Al7075 with B_4C, ZrO_2, and Graphite Additions

3.4. Compressive Fractography

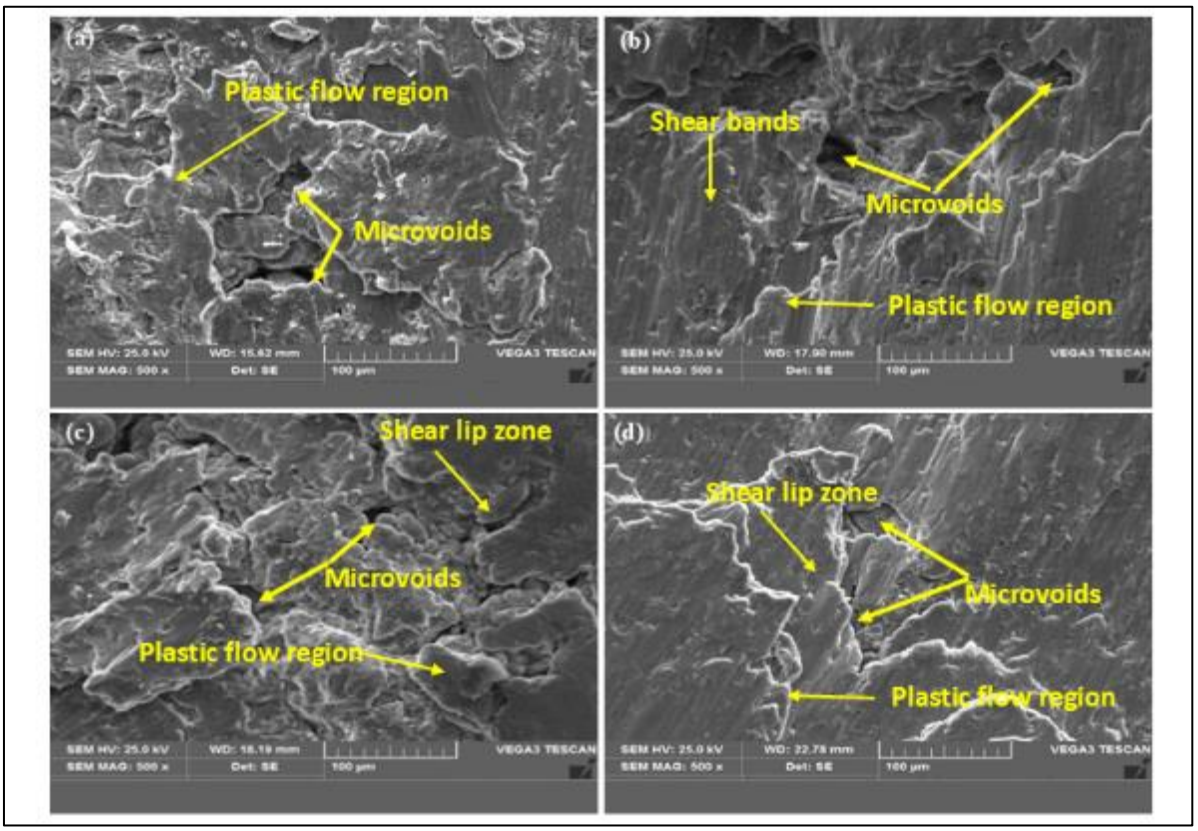

Figure 12 SEM micrographs of compressive fracture surfaces of (a) Al7075 alloy, (b) Al7075–3 wt.% B_4C, (c) Al7075–3 wt.% ZrO_2, and (d) Al7075–3 wt.% Gr composites.

The SEM fractography shown in Figure 12 demonstrate how the type of reinforcement has a significant impact on the compressive fracture behaviour of Al7075. Under compressive loading, the unreinforced Al7075 alloy (Fig. 12a) shows large plastic flow regions with lots of microvoids, suggesting a primarily ductile deformation mechanism. The Al7075 3wt.% B_4C composite (Fig. 12b) exhibits noticeable shear bands with decreased plastic flow, indicating that the hard

B_4C particles successfully limit matrix deformation and improve load-bearing capacity through effective stress transfer. The fracture surface of the Al7075 3wt.% ZrO_2 composite (Fig. 12c) exhibits shear lip zones along with localised microvoids and plastic flow, indicating a mixed-mode fracture behaviour controlled by particle–matrix interactions and localised plastic deformation. On the other hand, because graphite is soft and layered, the Al7075 3wt.% Gr composite (Fig. 12d) exhibits noticeable shear lip zones with extensive plastic flow and microvoid coalescence, suggesting improved energy absorption and ductile behaviour. Overall, Figure 12(a–d) shows that in Al7075 composites, B4C mainly improves compressive strength and rigidity, ZrO_2 offers a balance between strength and toughness, and graphite encourages ductility and damage tolerance.

3.5. Impact Fractography

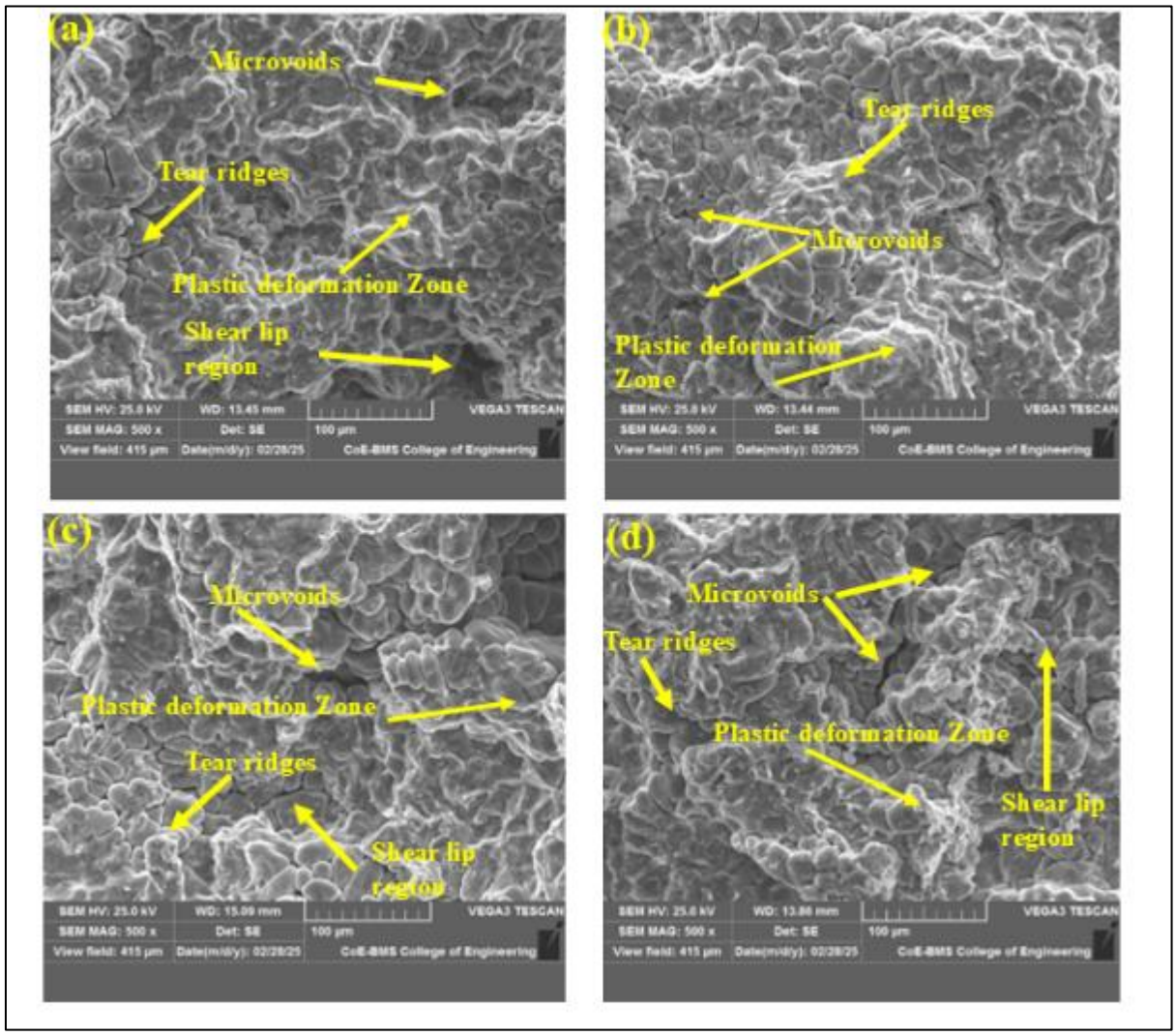

Figure 13 SEM micrographs of Impact fracture surfaces of (a) Al7075 alloy, (b) Al7075–3 wt.% B_4C, (c) Al7075–3 wt.% ZrO_2, and (d) Al7075–3 wt.% Gr composites

The SEM micrographs of impact-fractured surfaces of (a) unreinforced Al7075 alloy, (b) Al7075–3 wt.% B_4C, (c) Al7075–3 wt.% ZrO_2, and (d) Al7075–3 wt.% Gr composites are shown in Figure 13, demonstrating the unique impact of individual reinforcements on impact failure behaviour. A highly ductile fracture mechanism under impact loading is confirmed by the Al7075 alloy (Fig. 13a), which displays extensive plastic deformation zones with well-developed tear ridges, microvoids, and prominent shear lip regions. The fracture surface of the Al7075 3wt.% B_4C composite (Fig. 13b) exhibits comparatively finer microvoids, less plastic deformation, and noticeable tear ridges, suggesting limited matrix flow and enhanced resistance to impact-induced deformation because of the hard B_4C particles.

Microvoid coalescence, tear ridges, and localised shear lip regions are all present in the Al7075 3wt.% ZrO_2 composite (Fig. 13c), indicating a mixed-mode fracture behaviour controlled by localised plastic deformation and effective

particle–matrix interaction. Improved impact strength without undue brittleness is a result of this balanced fracture response. On the other hand, the Al7075 3wt.% Gr composite (Fig. 13d) shows many microvoids, well-developed shear lip regions, and large plastic deformation zones, all of which are signs of improved energy absorption and ductile fracture behaviour. Graphite's layered structure slows the spread of cracks under impact loading by promoting interfacial sliding and crack blunting. Overall, shows that graphite greatly increases impact toughness through ductile deformation mechanisms, ZrO_2 offers a balanced strength–toughness response, and B_4C improves impact resistance by limiting plastic flow.

4. Conclusion

This study demonstrated that Al-7075 composites reinforced with 3 wt.% B_4C, graphite, and ZrO_2 can be successfully fabricated using a two-step stir-casting technique, achieving uniform reinforcement dispersion and strong matrix–particle interfacial bonding. Mechanical evaluation revealed that reinforcement type plays a critical role in governing performance: B_4C provided the highest improvement in hardness and tensile strength due to its high stiffness, effective load transfer, and restriction of plastic deformation; ZrO_2 offered a balanced enhancement in strength and toughness through localized plastic deformation and particle–matrix interactions; and graphite reduced hardness but significantly improved ductility and impact toughness by promoting crack deflection and energy absorption. Compressive and impact fractographic analyses corroborated these trends, with B_4C-reinforced composites exhibiting limited plastic flow and brittle-dominant fracture, ZrO_2-reinforced composites showing mixed-mode fracture behaviour, and graphite-reinforced composites displaying extensive plastic deformation and superior damage tolerance. Overall, the findings highlight that appropriate reinforcement selection enables tailored design of Al-7075 composites for strength-critical or impact-resistant applications in aerospace, automotive, and defence sectors.

Compliance with ethical standards

Disclosure of conflict of interest

No conflict of interest to be disclosed.

Author Contribution

Sampath Kumar R – Manuscript Draft, Conceptualization, Experiments, Testing & characterization, and Analysis, Manuscript-updating, H C Chittappa Results Analysis, Supervision

References

[1] RinoJJ,ChandramohanD, SucitharanKS, JebinVD. An overview on development of aluminium metal matrix composites with hybrid reinforcement. IJSR India Online ISSN 2012: 2319–7064.

[2] Ezhil, S., Vannan., Paul, S. and Vizhian (2014). Microstructure and mechanical properties of as cast aluminium alloy 7075-basalt dispersed metal matrix composites. Journal of Minerals and Materials Characterization and Engineering, 2, pp. 182–193.

[3] Baradeshwaran and Elaya, Perumal (2014). Study on mechanical and wear properties of Al7075-Al2O3-Graphite hybrid composites. Composites Part B: Engineering, 56, pp. 472-476.

[4] Sharma, S., Kini, A., Gowri, Shankar, T, C. and Raja, Rakesh, H. (2018). Tensile fractography of artificially aged Al6061-B4C composites. Journal of Mechanical Engineering and Sciences, 12, 3, pp. 3866–3875.

[5] Bekir, Sadik, Unlu (2008). Investigation of tribological and mechanical properties Al2O3-SiC reinforced Al composites manufactured by casting or PM method. Materials & Design, 29, 10, pp. 2002–2008.

[6] Nagaral, M., Hiremath, V., Auradi, V. and Kori, S, A. (2018). Influence of two stage stir casting process on mechanical characterization of AA2014-ZrO2 nano composites. Transactions of the Indian Institute of Metals, 71, pp. 2845-2850.

[7] Wang, W., An, D., Fan, Y., Zhao, X., Wang, X., Ma, R. and Li, Q. (2018). Microstructure and tribological properties of SiC matrix composites infiltrated with an aluminium alloy. Tribology International, 120, pp. 369–375.

[8] V. Bharath, V. Auradi, M. Nagaral, Fractographic characterization of Al2O3p particulates reinforced Al2014 alloy composites subjected to tensile loading, Frattura ed IntegritàStrutturale 15 (2021) 14–23 9.

[9] S.B. Boppana, S. Dayanand, B. Vedashantha Murthy, M.Nagaral, A. Telagu, V. Kumar, V. Auradi, Development and mechanical characterisation of Al6061-Al2O3-graphene hybrid metal matrix composites, J. Compos. Sci. 5 (2021) 155

[10] Jung J, Kang S. Advances in manufacturing boron carbide–aluminum composites. J Am Ceram Soc 2004;87(1):47–54.

[11] Zhu X, Dong H, Lu K. Coating different thickness nickel–boron nanolayers onto boroncarbide particles. Surf Coat Technol 2008; 202:2927–34.

[12] Shrestha NK, Kawai M, Saji T. Co-deposition of B4C particles and nickel under the influence of a redox-active surfactant and anti-wear property of the coatings. Surf Coat Technol 2005; 200:2414–9.

[13] N Nagaraj, KV Mahendra, Madeva Nagaral. Investigations on mechanical behaviour of micro graphite particulates reinforced Al-7Si alloy composites. IOP conference series: materials science and engineering, 310, 1, 2018, 01211.

[14] Vida Khalili, Akbar Heidarzadeh , Sajjad Moslemi , Leila Fathyunes "Production of Al6061 matrix composites with ZrO2 ceramic reinforcement using a low-cost stir casting technique: Microstructure, mechanical properties, and electrochemical behavior'' journal of materials research and technology 2020;9(6):15072-15086.

[15] Chandana Sri, S. Saravanamurugan, A. Shanmugasundaram, Subinaya Mohapatra "Effect of SiC and Gr particles on the mechanical properties and dynamic characteristics of AA 7075 hybrid metal matrix composite'' Materials Today: Proceedings 2020.

[16] Bharath Vedashantha Murthy, Virupaxi Auradi, Madeva Nagaral, Manjunath Vatnalmath, Nagaraj Namdev, Chandrashekar Anjinappa, Shanawaz Patil, Abdul Razak, Abdullah H Alsabhan, Shamshad Alam, Mohammad Obaid Qamar. Al2014–alumina aerospace composites: particle size impacts on microstructure, mechanical, fractography, and wear characteristics. ACS Omega, 8, 4, 2023, pp. 13444-13455.

[17] Mondal S. Aluminum or its alloy matrix hybrid nanocomposites. Met Mater Int 2021;27:2188–204. [5] Kaushik Y, Jawalkar

[18] Sujith SV, Kim H, Mulik RS, Park H, Lee J. Synergistic effect of in-situ Al-7075/ Al3Ti metal matrix composites prepared via stir-assisted ultrasonic melt processing under dynamic nucleation. Met Mater Int 2022;28(9):2288–303.

[19] R. Ramesh, S. Suresh Kumar, and S. Gowrishankar, "Productionand characterization of aluminium metal matrix composite reinforced with Al3Ni by stir and squeeze casting," Applied Mechanics and Materials, vol. 766-767, pp. 315–319, 2015.

[20] J. Singh, A. Chuan, Fabrication characteristics and tensile strength of novel Al2024-SiC-red mud composites processing via stir casting route, Trans. Nonferrous Metals Soc. China27 (2017) 2573–2586.

[21] Nagaral M, Auradi V, Kori SA (2014) Dry sliding wear behaviour of graphite particulate reinforced Al6061 alloy composite materials 170-174; 592-594.

[22] M. Nagaral, R.G. Deshapande, V. Auradi, S.B. Boppana, S. Dayanand, M.R. Anilkumar, Mechanical and wear characterization of ceramic boron carbide-reinforced Al2024 alloy metal composites, J. Bio- Tribo-Corros. 7 (2021) 1–12

[23] Standard Test Methods for Tension Testing of Metallic Materials, ASTM E8, 10.1520/E0008_E0008M-22

[24] Nagaral, M., Shivananda, B. K., Auradi, V., & Kori, S. A. (2016, September). Effect of SiC and graphite particulates addition on wear behaviour of Al2219 alloy hybrid composites. In IOP Conference Series: Materials Science and Engineering (Vol. 149, No. 1, p. 012108). IOP Publishing.

[25] Kotresha Mydur , Mahendra Kumar S., Madeva Nagaral et al " Microstructure, physical, tensile and wear behaviour of B4C particles reinforced Al7010 alloy composites" Manufacturing Rev. 10, 3 (2023).

[26] Rashmi P Shetty, T Hemanth Raju, Madeva Nagaral, Nithin Kumar, V Auradi. Effect of B_4C Particles Addition on the Mechanical, Tensile Fracture and Wear Behavior of Al7075 Alloy Composites. Journal of Bio-and Tribo-Corrosion, 10, 2, 2024, 32.